Solution Properties of Xanthan. 1. Dynamic and Static Light Scattering from Native and Modified Xanthans in Dilute Solutions

T. Coviello,[‡] K. Kajiwara,[§] W. Burchard,*[†] M. Dentini,[‡] and V. Crescenzi[‡]

Institute of Macromolecular Chemistry, University of Freiburg, D-7800 Freiburg, FRG.
Received April 1, 1986

ABSTRACT: The chain stiffness of "native" xanthan (NX) (commercial product of Kelco Inc.), pyruvate-free xanthan (PFX), and acetyl-free xanthan (AFX) has been determined from static light scattering measurements. The Kuhn lengths were determined as being l_K = 255 ± 15 nm for NX, 310 ± 40 nm for PFX, and 198 ± 13 for AFX by employing a recently suggested technique of evaluating the angular dependence of the scattered light. The radii of gyration were calculated with these data from the Benoît–Doty equation for polydisperse chains and found to agree within 0.5% of the measured radii. The hydrodynamic radii were derived from measurements of the translational diffusion coefficients by means of dynamic light scattering. Using the mentioned Kuhn lengths and assuming a chain thickness of d = 2.2 nm, we calculated the hydrodynamic radii by the theory of Yamakawa and Fujii. The values were found to be in agreement with the measurement for PFX but about 18% lower for NX and even still 8% lower if d = 5 nm is assumed; for AFX agreement was found with d = 3.3 nm. The time correlation functions (TFC) measured at various angles can be cast into a general shape function $\mathcal{S}(\Gamma t)$, which is only dependent on Γt, where Γ is the first cumulant of the individual TCF's. This shape function follows that of a rigid rod for small Γt and approaches the shape function of a flexible chain for larger Γt, as can be expected for a wormlike chain. Examination of the angular dependence of the first cumulant again reveals intermediate behavior to rigid rods and flexible chains.

Introduction

The bacterial polysaccharide xanthan (see structure in Figure 1), produced by *Xanthomonas campestris*, has aroused much interest because of its unique solution properties. Most striking, for instance, is the very high viscosity of dilute solutions, which is a strong indication for a pronounced chain rigidity. Paradossi and Brant[1] tried to determine the shape of the molecules by common static light scattering. These measurements indeed exhibit the typical rodlike asymptotic scattering behavior of the particle scattering factor. The authors came to the conclusion that xanthan is a double-stranded chain. Later these data were used by Schmidt et al.[2] for an estimation of the Kuhn segment length l_K, applying a procedure based on a theory by Koyama,[3] where a value of l_K = 200 ± 20 nm was obtained. This is an extraordinarily high value compared to that for cellulose derivatives, with l_K = 20 ± 5 nm.[4-6] Nevertheless, xanthan is not a rigid rod as was often assumed.

The immense increase of chain stiffness relative to the common cellulose derivatives (xanthan has a cellulose backbone) raises the question of which factors could be responsible for such a drastic reduction in xanthan chain flexibility. Recently, Dentini et al.[7] carried out optical activity measurements at various temperatures with native xanthan and three modified xanthans, where the pyruvate group, the acetate group, or both were removed. They noticed that the helix–coil transition was shifted toward higher temperatures when the pyruvate group was cleaved, while it was shifted toward lower temperatures when the acetyl group was removed. These observations suggested a stabilization of the ordered structure of the xanthan chain if the charged pyruvate group is absent and to the contrary, a destabilization when the acetyl group is not present.

These results stimulated the present study on various xanthan samples by static and dynamic light scattering in an attempt to establish a connection between the ordered structure stabilization and the Kuhn segment length, which characterizes the stiffness of the polymer chains.

Experimental Section

1. Sample Preparation. The "native" xanthan (xanthan I), supplied by Kelco Inc. (Keltrol F), was previously purified[7] as described by Holzwarth[8] and then converted into the Na form. In one sample of a different batch (xanthan II) the pyruvate groups were cleaved by heating a 0.4% xanthan II solution containing 0.1 M NaCl and 2 × 10^{-3} M oxalic acid at 95 °C for 2 h. The solution was then neutralized at room temperature with stirring, dialyzed against double-distilled water, filtered, and freeze-dried.

The *O*-acetyl groups were removed by allowing the xanthan II solutions (0.2% in 0.1 M NaCl) to stand for 3 h in a 2.5 × 10^{-3} M NaOH solution at room temperature, followed by neutralization and by dialysis.[9] All solutions were then filtered and freeze-dried.

2. Preparation of Solutions for Light Scattering. Stock solutions for light scattering were prepared by dissolving the polymer in 0.1 M NaCl, and these solutions were then heated (T = 116 °C) under pressure for approximately 30 min. This procedure proved to be essential, since only after this treatment were aggregates broken up and very clear solutions obtained which gave reproducible light scattering results. After that, the stock solutions were dialyzed against aqueous 0.1 M NaCl for 5 days in a special cell at constant volume, and the dilution was then made with the dialyzed solvent. The solutions of suitable concentrations (0.4 × 10^{-3} to 1.0 × 10^{-3} g/mL) were heated for about 10 min under pressure (T = 160 °C), which was effective in achieving reproducible results, and then filtered through 0.45-μm Millipore sterilized one-way filters directly into the light scattering cells. We wish to point out that even the stock solutions have concentrations *below* the coil overlap. Behavior in the semidilute regime has been studied separately and will be reported in part 2 of this investigation.[40]

Rinaudo et al.[10] reported cleavage of pyruvate groups after keeping xanthan for 2 days at 95 °C. Such cleavage appears unlikely in our case since the samples were heated at most for 0.5 h, and after such a short time, Rinaudo et al. found no detectable change in the pyruvate content.

3. Light Scattering. Static and dynamic light scattering measurements were carried out simultaneously in the angular range 30–140° at 20 °C with the red line (λ_0 = 647.1 nm) of a Kr ion laser (Spectra Physics, Model Kr 164-08) (NX and PFX) and the blue line (λ_0 = 488 nm) of an Ar ion laser (Spectra Physics, Model Ar 165-06) (AFX). The details of the instrument and the

[†] Institute of Macromolecular Chemistry, University of Freiburg, FRG.
[‡] Dipartimento di Chimica, Università di Roma "La Sapienza", Italy.
[§] Institute for Chemical Research, Kyoto University, Japan.

0024-9297/86/2219-2826$01.50/0

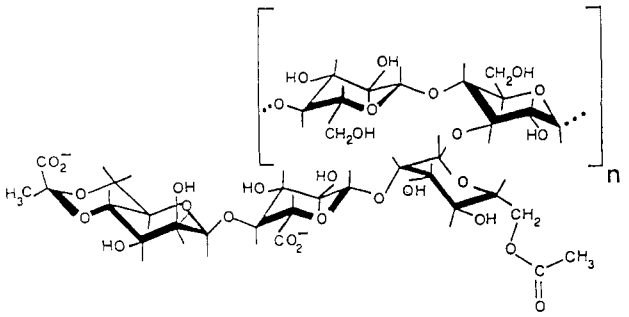

Figure 1. Chemical structure of xanthan.

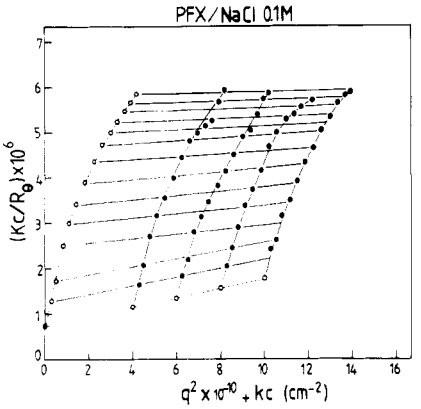

Figure 2. Static Zimm plot of the light scattering measurements from a pyruvate-free xanthan (PFX) in NaCl 0.1 M at 20 °C; c = 0.4 × 10^{-3}, 0.6 × 10^{-3}, 0.8 × 10^{-3}, and 1.0 × 10^{-3} g cm^{-3}.

Table I
Molecular Weight M_w, Radii of Gyration $\langle S^2\rangle_z^{1/2}$, Second Virial Coefficient A_2, Measured and Calculated Linear Mass Density $M = M/L$, and the Ratio of Both Quantities, Indicating the Number of Lateral Strands

parameter	NX	PFX	AFX
$M_w \times 10^{-6}$, dalton	2.94	1.37	1.77
$(\langle S^2\rangle_z^{1/2})_{exptl}$, nm	289.5	240.8	210.0
$(\langle S^2\rangle_z^{1/2})_{calcd}$, nm	298.1	242.3	213.6
$A_2 \times 10^4$, (cm³ mol)/g²	4.94	5.22	6.00
$(M/L)_{exptl}$, dalton/nm	1830 ± 80	1240 ± 160	1623 ± 48
$(M/L)_{theor}$, dalton/nm	899[a]	835[a]	860[a]
	(1033)[b]	(954)[b]	(988)[b]
$(M/L)_{exptl}/(M/L)_{theor}$	2.0 ± 0.1[a]	1.5 ± 0.2[a]	1.9 ± 0.1[a]
	(1.8 ± 0.1)[b]	(1.3 ± 0.2)[b]	(1.7 ± 0.1)[b]

[a] Calculated with l_0 = 1.08 nm. [b] Calculated with l_0 = 0.94 nm.

data evaluation procedure are given in ref 11.

Results

The static and dynamic light scattering measurements were performed at 20 °C with four concentrations in the range (0.4–1.0) × 10^{-3} g/mL. The static light scattering data were evaluated first from common Zimm plots. One of them is shown in Figure 2. From these plots M_w, $\langle S^2\rangle_z^{1/2} \equiv R_g$, and A_2 were obtained (Table I). The third virial coefficient is very low for all samples. The angular dependences in the Zimm plots at large q (=$(4\pi/\lambda)$ sin $(\theta/2)$) show clear deviations from a straight line toward lower values that are typical for stiff or rodlike molecules.[12,13]

The same light scattering data were plotted as qR_θ/Kc against qR_{gc} (where $R_{gc} \equiv \langle S^2\rangle_c^{1/2}$ is the apparent radius of gyration at concentration c) to further examine the structure factors. In the following, this graph will be called a Holtzer plot.[2,14] (See Figure 3.) At large q all curves appear to reach a constant plateau of the same value. Such

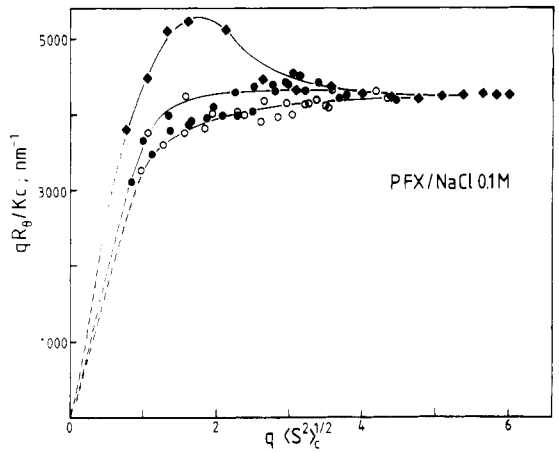

Figure 3. Holtzer plot of the particle scattering factor for the same PFX as in Figure 2 in 0.1 M NaCl at 20 °C: lowest curve, c = 1.0 × 10^{-3} g cm^{-3}; intermediate curve, c = 0.4 × 10^{-3} g cm^{-3}; extrapolated values for c = 0.

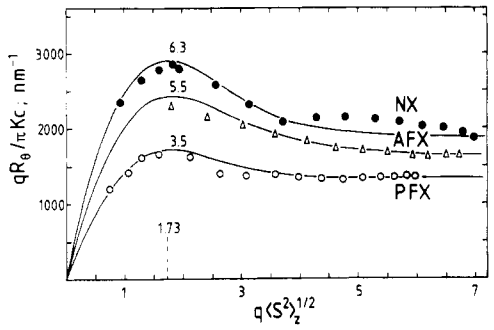

Figure 4. Holtzer plots of the particle scattering factor (at c = 0) for NX, AFX, and PFX. The numbers on the curves denote the number of Kuhn segments per chain; the full lines were calculated with the Koyama theory for polydisperse chains, M_w/M_n = 2, with the indicated number of Kuhn segments and the linear mass densities given in Table I.

an asymptotic plateau is characteristic of rigid rods,[14] and its magnitude is

$$qR_\theta/(Kc) \rightarrow \pi M_L \qquad (1)$$

where M_L is the linear mass density, which is the mass of a rod section per nanometer of length. The values found are given in Table I together with the theoretical values for the single-stranded chains. For lower q values the curves gradually go to zero, and this downturn occurs earlier for the higher concentrations. Thus the particle scattering factors are fairly strongly concentration dependent and have to be extrapolated toward zero concentration. Using the extrapolated curves obtained from the Zimm plots, one now finds curves that show a clear maximum before the constant plateau is reached. The three limiting curves of native (NX), pyruvate-free (PFX), and acetyl-free (AFX) xanthans are again plotted in Figure 4 as function of $qR_g = u$. In all cases the maximum is found at the same value of u^* = 1.73, as expected for polydisperse (M_w/M_n = 2) samples,[2] but the maximum for NX is more pronounced than for PFX. Recently, we have shown[2] that the height of the maximum divided by the height of the plateau is a measure for the number of Kuhn segments per chain, where the length of the Kuhn segment is a characteristic parameter of chain stiffness. Details of the analysis are given in the Discussion.

For the determination of the translational diffusion coefficients we carried out dynamic light scattering, where the scattering intensity time correlation function (TCF) $G_2(t) = \langle i(0)i(t)\rangle$ is measured. ($i(0)$ and $i(t)$ denote the

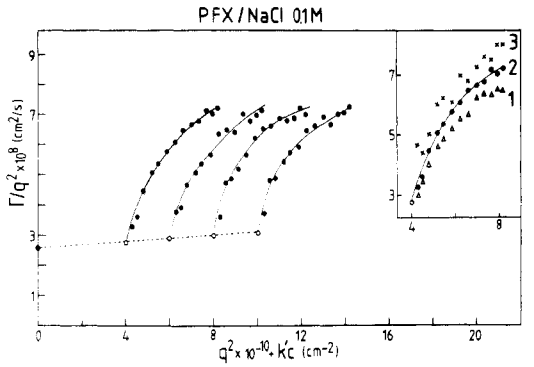

Figure 5. Dynamic Zimm plot of the light scattering measurements from PFX in 0.1 M NaCl at 20 °C. (Insert) D_{app} against $q^2 \times 10^{-10} + Kc$ for $c = 0.4 \times 10^{-3}$ g cm^{-3}: curve 1 (△) two-cumulant fit with 80 channels; curve 2 (●) three-cumulant fit with 80 channels; curve 3 (×) three-cumulant fit with 25 channels.

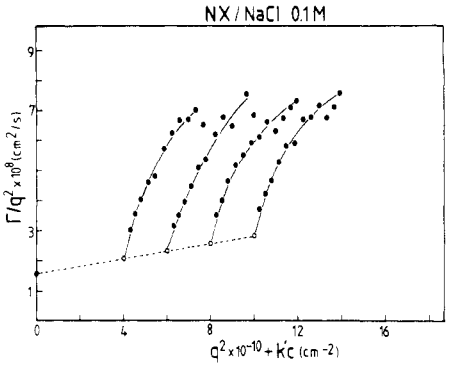

Figure 6. Dynamic Zimm plot of the light scattering measurements from NX in 0.1 M NaCl at 20 °C.

scattering intensities at zero time and at a delay time t.) This intensity TCF is related to the normalized electric field TCF, $g_1(t)$, as

$$G_2(t) = A + Bg_1(t)^2 \tag{2}$$

with

$$g_1(t) = |\langle E^*(0)E(t)\rangle|/|\langle E^*(0)E(0)\rangle| \tag{3}$$

where $E(0)$ and $E(t)$ are the electric field amplitudes at zero time and delay time t and where the star denotes the conjugate complex quantity. The TCF $G_2(t)$ shows an exponential-like decay to a base line A, and B is an efficiency parameter that is characteristic of the signal/noise ratio. Because of the exponential-like decay for $g_1(t)$ one can try to analyze the TCF via a cumulant expansion given by[16]

$$\ln g_1(t) = -\Gamma_1 t + \Gamma_2/2!t^2 - \Gamma_3/3!t^3 + \ldots \tag{4}$$

where $\Gamma = \Gamma_1, \Gamma_2, \Gamma_3, \ldots$ are the first, second, third, ... cumulants. The theory of dynamic light scattering proves[15] for the first cumulant measured at a certain concentration that

$$\Gamma_1/q^2 = D_c(q) \tag{5}$$

where $D_c(q)$ is an apparent, angular-dependent diffusion coefficient at the concentration c. We tried to determine this diffusion coefficient from the initial slope of the TCF $g_1(t)$ that were measured at the same scattering angles and concentrations as for the static light scattering.

The estimation of the initial slope of the TCF involved difficulties for the PFX sample since deviation from a single-exponential behavior started already at rather short delay times. We applied a two-cumulant and a three-cumulant fit and also varied the number of points used for the fit. The insert in Figure 5 shows the result with lowest concentration for PFX.

Curve 1 represents the apparent diffusion coefficient obtained from a two-cumulant fit of the TCF when all 80 channels were taken into account, curve 2 shows the corresponding three-cumulant fit, and curve 3 gives the result of a three-cumulant fit where only the first 25 channels were used. In principle, curve 3 should give the best result but, because of the limiting number of points of measurement, the spread of error becomes too large for PFX to allow an accurate extrapolation to zero angle. It turned out that the choice of a small number of channels yielded good results only in rare cases. We always carried out fits with 25 and 80 channels and then took that fit which gave consistent results. This point has to be kept in mind in the discussion of the parameter C defined in the next section. The difficulties mentioned did not occur with the native and the acetyl-free xanthans.

Table II
Translational Diffusion Coefficient, D_z, Hydrodynamic Radius R_H, $\rho = R_g/R_H$, and the Coefficients k_d and k_{f0} Defined by Eq 6 and 14

parameter	NX	PFX	AFX
$D_z \times 10^8$, cm²/s	1.55	2.60	2.60
$(\langle R_H\rangle_z)_{exptl}$, nm	137.2	81.5	81.5
$(\langle R_H\rangle_z)_{calcd}$, nm	112.8[a]	85.4[a]	76.81[a]
	126.4[b]		86.88[b]
			81.47[c]
ρ_{exptl}	2.17	2.95	2.58
k_d, mL/g	873	296	231
k_{f0}	0.92	1.14	2.43

[a] From Yamakawa–Fujii theory[24b] with $d = 2.2$ nm. [b] From Yamakawa–Fujii theory[24b] with $d = 5.0$ nm. [c] From Yamakawa–Fujii theory[24b] with $d = 3.3$ nm.

Figures 5 and 6 show the dynamic Zimm plots[17] for PFX and NX, where $D_{app}(q)$ is plotted against $q^2 + kc$. From these Zimm plots one obtains the translational diffusion coefficient at zero concentration D_{0z} as the intercept and a parameter k_D from the slope of the curve $q = 0$ which describes the concentration dependence of the diffusion coefficient according to the relationship

$$D_c = D_{0z}(1 + k_D c) \tag{6}$$

Finally, from the initial slope of the curve $c = 0$ (not shown) the structure-dependent parameter C is found according to the equation

$$D_c(q) = D_c(1 + C\langle S^2\rangle q^2 - \ldots) \tag{7}$$

The results are listed in Table II together with other structure-relevant parameters.

Discussion

Chain Stiffness. The scattering curves at infinite dilution in the Holtzer plots (Figure 4) exhibit a shape characteristic of semiflexible or wormlike chain molecules.[2] They may be analyzed as follows.

(1) From the ratio of the maximum value to that of the plateau, the number of Kuhn segments N_K per molecule is obtained by using a relationship published by Schmidt et al., which is reproduced in Figure 7.

(2) The height of the plateau gives the linear mass density M_L, from which, together with the molecular weight M_w, one gets the contour length L_w

$$L_w = M_w/M_L \tag{8}$$

(3) The Kuhn length is then given by

$$l_K = L_w/N_K \tag{9}$$

The data are collected in Table III.

For a check of the Kuhn lengths thus obtained we calculated the radius of gyration assuming a most probable

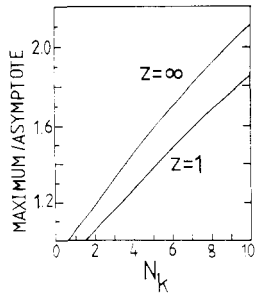

Figure 7. Plot of the height of the maximum to that of the asymptote for the curves in Figure 3 as function of the number of Kuhn segments.[2] ($z = \infty$ corresponds to $M_w/M_n = 1$ and $z = 1$ corresponds to $M_w/M_n = 2$.)

Table III
Melting Temperatures T_m (Salt-Free Solutions), Ratio of Measured and Calculated Linear Mass Density, Ratio of Maximum and Asymptote from the Holtzer Plot, Contour Lengths L_w, Number of Kuhn Lengths N_K, Length of Kuhn Segments l_K, and Parameter C (Eq 7)

parameter	NX	PFX	AFX
T_m, °C	45	60	30
$(M/L)_{exptl}/(M/L)_{theor}$	2.04 ± 0.08	1.49 ± 0.19	1.89 ± 0.05
max/asymptote	1.52 ± 0.07	1.21 ± 0.03	1.42 ± 0.04
L_w, nm	1609 ± 70	1027 ± 49	1087 ± 31
N_K	6.3 ± 0.6	3.5 ± 0.4	5.5 ± 0.4
l_K nm	255 ± 15	310 ± 40	198 ± 13
C	0.22	0.08	0.09

Schulz–Flory distribution and using the formula by Benoît and Doty[18] for the wormlike chains. This relationship for the most probable distribution takes the simple form[19]

$$\langle S^2\rangle_z = (l_K^2/4)N_K^2/(1 + N_K) \qquad (10)$$

The calculated radii of gyration agree closely with the measured ones, as may be recognized from Table I.

In Figure 8 our radii of gyration are plotted on a double-logarithmic scale together with the data of Paradossi and Brant,[2] obtained from degraded NX samples. Our points fit very satisfactorily their results and also those of Sato et al.[21] We also calculated the curves for polydisperse double-stranded chains with Kuhn lengths of 300, 200, and 100 nm. Evidently no clear determination of the Kuhn length is possible for short chains, because in this region the chains behave similarly to rod molecules. Deviations from rod behavior become noticeable in experiments only for longer chains when the number of Kuhn segments exceeds $N_K = 2$. Note that the measurements cannot be fitted with monodisperse double-stranded chains, even if $l_K = 300$ nm is assumed.

The Kuhn length of 255 ± 15 nm obtained in our study for NX agrees closely with results by Sato et al.,[20,21] who obtained $l_K = 240$ nm from measurements of the radius of gyration as function of M_w, applying the Benoît–Doty formula. They also found good agreement with their intrinsic viscosity data when applying the Yoshizaki–Yamakawa[22] theory of wormlike helices, assuming a thickness of $d = 2.2$ nm.[20,21] Müller[23] fitted his viscosity measurements of native xanthans with the Yamakawa–Fujii[24a] theory and found the much lower value $l_K = 100$ nm when using $d = 1.9$ nm but he assumed a single-stranded chain, which reduces the Kuhn length at least by a factor of 2. However, NX and AFX are double-stranded, as demonstrated in Figure 4 and by Sato et al.[20,21] The xanthans thus belong among the most rigid polymers. Only schizophyllan[25] has a larger Kuhn length ($l_K = 390 \pm 10$ nm); comparable values are found with collagen[26] ($l_K = 260$ nm) while DNA is, with $l_K = 120$ nm, considerably more flexible.[27] We also find a good agreement for the linear mass density $M_L = 1830 \pm 80$ dalton nm^{-1} with that of Sato et al. ($M_L = 1940 \pm 40$ dalton nm^{-1}); in the present study this quantity was obtained from the plateau of the Holtzer plot, while Sato et al. derived a value of $M_L = 1940 \pm 40$ dalton nm^{-1} from $\langle S^2\rangle_z^{1/2} = (l/12^{1/2})(M_w/M_L)$, which holds for monodisperse rigid rods and which they assumed to be realistic for short xanthans.[22]

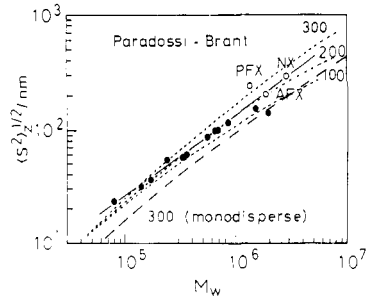

Figure 8. Molecular weight dependence of the radius of gyration $\langle S^2\rangle_z^{1/2}$ for various xanthan fractions: (●) Paradossi and Brant;[1] (○) present work; (---) calculated curves for polydisperse chains assuming Kuhn segment lengths of 100, 200, and 300 nm, respectively; (– – –) calculated for monodisperse chains with a Kuhn segment length of 300 nm (a double-stranded chain was assumed).

According to our findings, NX and AFX behave like a double-stranded chain, which is in good agreement with results of other laboratories.[1,20,21,41] PFX, however, shows a lower linear mass density M_L (see Figure 4) indicating 1.5 strands on the average. Simultaneously, the Kuhn length increases from 255 nm for NX to 310 nm for PFX. Evidently the ordered structure of the modified xanthan becomes more stabilized, as was already found from optical activity measurements at various temperatures[7] (Table III). The Kuhn length of AFX, on the other hand, is smaller than for NX, and this is again in agreement with the lower melting temperature. The lower mass per unit length for PFX gives evidence for a single-stranded chain. A factor 1.5 may result for different reasons. First, we have to recall that only 85% of the pyruvate groups have been removed. Therefore, a number of double-stranded sections may still exist. Under such conditions two helical segments of one chain may form double strands with *two* other rather than with only *one* other chain, and this would result in a partial association and an increase of the overall molecular weight. This in turn gives rise to a longer apparent linear mass density. The increase of chain rigidity for the essentially single-stranded PFX chain is somewhat unexpected. At present we cannot offer a conclusive interpretation but can merely speculate on the reasons as follows: The side chain may possibly stabilize the structure by winding around the backbone. This may make the terminal OH group in C4 lie behind the acetyl group of the first sugar, thus forming a special interaction. Finally, we have to remark that a repeat unit length of $l_0 = 1.08$ nm was taken as the basis for the calculation of M_L, which corresponds to a stretched cellulose backbone. The corresponding length of NX in the crystalline state was found to be $l_0 = 0.94$ nm, which gives the data in parentheses in Table I.

Hydrodynamic Radius and Related Parameters. Next, the hydrodynamic radius R_H may be calculated and compared with those obtained from measurements of the translational diffusion coefficient, making use of the Stokes–Einstein relationship.

$$R_{Hz} = kT/(6\pi\eta_0 D_z) \qquad (11)$$

This hydrodynamic radius can be calculated from a theory by Yamakawa and Fujii,[24b] where two relevant points have to be kept in mind.

Table IV
Polydispersity Correction Factors $K(m)$ in Eq 12 for the Hydrodynamic Radius according to Ref 28

M_w/M_n	m	$K(m)$
2.0	1	1.067
1.5	2	1.046
1.333	3	1.036
1.25	4	1.029
1.20	5	1.024
1.167	6	1.021
1.143	7	1.020
1.0	∞	1.000

(1) The equations, which are not reproduced here, contain as an additional parameter the thickness d of the chain. This thickness, however, is introduced in this theory for mathematical reasons to avoid a singularity in integration. Therefore, the parameter d has to be considered as an adjustable parameter and not as an ad hoc physical parameter.

(2) Fujii and Yamakawa derived an equation only for monodisperse chains. To include polydispersity, tedious numerical integrations have to be performed. This was done by Schmidt.[19] He found that the influence of polydispersity on rigid and semiflexible chains is very close to that on flexible chains, which for distributions of the Schulz–Zimm type is given by the equation[28]

$$\langle 1/R_H \rangle_z = \langle 1/R_H \rangle / K(m) \tag{12}$$

where

$$m = 1/(M_w/M_n - 1) \tag{13}$$

The polydispersity correction factor $K(m)$ (defined as $K_{pw}(\infty)/K_{pw}(m)$ in ref 28) has been calculated earlier and is listed for special polydispersities in Table IV.

For a Schulz–Flory most probable distribution one has $m = 1$, and the correction term in eq 12 is 1.067. The values for the hydrodynamic radii listed in Table II were calculated with the indicated diameter, applying the polydispersity correction for a most probable distribution and using the Yamakawa–Fujii theory.[24b,29]

In a previous paper we have shown that the parameters $\rho = R_{gz}/R_{Hz}$ and C in eq 7 are characteristic of the architecture of macromolecules.[17b] The dependence of these two parameters on chain stiffness was calculated by Schmidt and Stockmayer.[19,30] The ρ values of the xanthans are in all cases about 2 times lower than predicted by Schmidt[19] for an axial ratio of $L_w/d = 10^4$ (Table II). The actual ratio is, however, $L_w/d = 700$ for NX and a little higher for PFX, and this will make the discrepancy even larger. For the C parameter (Table III) we find for NX a value that is only slightly smaller than estimated for a polydisperse chain, but for PFX the measured value is even lower than predicted for a monodisperse chain (see Figure 3 in ref 19). Note, however, the difficulties in determining the slope in Figure 5 for PFX, which did not occur for NX and AFX.

Another parameter of interest is the k_{f0} value,[31] which is derived from the second virial coefficient, and the constant k_d, describing the concentration dependence of the translational diffusion coefficient

$$k_{f0} = k_f M/(N_A V_h) \tag{14}$$

where[31b]

$$k_f = 2A_2M - k_d + \upsilon_2 \tag{15}$$

and

$$V_h = (4\pi/3)R_H^3 \tag{16}$$

with υ_2 being the partial specific volume of the polymer.

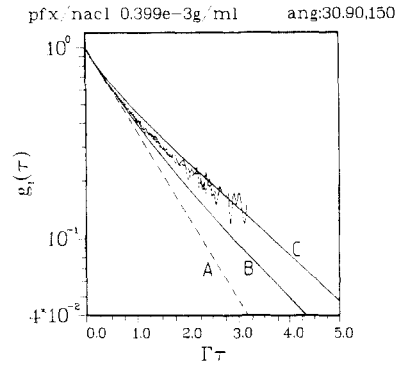

Figure 9. Shape function (scaled time correlation function) of PFX in 0.1 M NaCl at $c = 0.4 \times 10^{-3}$ g cm^{-3} for scattering angles of 30, 90, and 150°: (A) single exponential; (B) shape function of a rod;[33] (C) shape function of a flexible chain[34,35] (Zimm case, strong hydrodynamic interaction).

For flexible chains the k_{f0} parameter is a measure of coil interpenetration (a large value of about 7.0 indicates low interpenetration while $k_{f0} = 2.23$ is predicted for fully interpenetrating coils). No theory is available for rigid rods or wormlike chains. It is still of interest to observe that our values (Table II) are even lower than for the soft sphere and than that found by Schmidt[19] for the poly(γ-benzyl glutamate) (PBLG) chain of low molecular weight.

Shape Function of the Dynamic Structure Factor. In general, the TCF $g_1(t)$ can be written as a sum of exponentials[15]

$$g_1(t) = \exp(-Dq^2t)[A_0(q) + \sum_{n=1}^{\infty} A_n(q) \exp(-t/\tau_n)] \tag{17}$$

where D is the translational diffusion coefficient of the center of mass and τ_n is the relaxation time of the nth internal mode of motion. These internal modes include random motion of sections in a flexible chain as well as the rotational diffusion, i.e., tumbling of the chain. The $A_n(q)$ are angular-dependent amplitude factors of their modes, which were given by Pecora[15] for the ideally flexible chain and the infinitely thin rigid rod. Later, the calculations for the rod were completed by Wilcoxon and Schurr[32] and by Maeda and Fujime,[33] who took into consideration the anisotropy of diffusion for long rods of finite thickness.

The translational diffusion coefficient D decreases inversely with the contour length L. Thus, in the limit of $L \to \infty$, D goes to zero and the first exponential becomes unity. Furthermore, the expression in the square brackets approaches for both the flexible chain[34,35] and the rigid rod[36] a general shape function $\mathcal{S}(\Gamma t)$

$$\lim_{Lq \gg 1} g_1(t) = \mathcal{S}(\Gamma t) \tag{18}$$

which only depends on the first cumulant Γ. This Γ is the initial slope of $-\ln \mathcal{S}(\Gamma t)$ against t and is a complicated function of q. The shape function for the flexible chain with strong hydrodynamic interaction was first calculated by de Gennes in 1967[34] and reestablished by Akcasu et al.[35] The complicated formula is not reproduced here but the function is plotted in Figure 9 as curve C.

The corresponding shape factor of the rigid rod was recently calculated by Hallett, Nickel, and Craig[36] and is

$$\mathcal{S}(\Gamma t) = (\pi^{1/2}/2)(\text{erf}\ (x)/x) \exp(-x^2/3) \tag{19}$$

where

$$x = ((3/2)\Gamma t)^{1/2} \tag{20}$$

This function is curve B in Figure 9.

Since the TCFs of infinitely long chains and rods are general shape functions, we wondered whether a similar

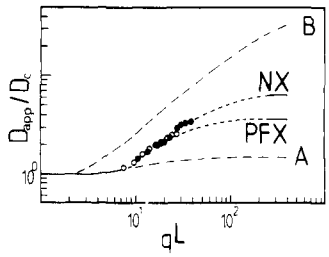

Figure 10. Normalized apparent diffusion coefficient against qL (L = contour length); D_c is the translational diffusion coefficient at concentration c and $q = 0$. (A) Theoretical curve for a rigid rod[37] assuming the contour length as the rod length; (B) theoretical curve for the "sliding-rod" model[37,39]; (●, ○) experimental points for NX and PFX at $c = 0.4 \times 10^{-3}$ g cm^{-3}. The bars indicate the limiting plateau values according to the Hammouda theory, assuming the Kuhn length as rigid rods.[37]

scaling with respect to Γ also holds for the semirigid xanthan chains. Figure 9 reveals that within experimental error such a general shape is found in the angular region of 30–150°.

The experimental curve follows for smaller values of Γt the shape function of the rod (curve B) but approaches for larger Γt that of the flexible chain (Zimm case, curve C).[35] Thus this shape function, for xanthan, exhibits behavior of a chain intermediate between a rod and a flexible chain. The experimental curve indicates the short-time behavior of a rod and the long-time behavior of a flexible chain. Indeed, the short relaxation time is determined by the rodlike segments, while the spectrum of the larger relaxation times is characteristic of the motion of longer more flexible subchains.

Angular Dependence of the First Cumulant. Finally, we compared the measured apparent diffusion coefficient (i.e., $D_{app}(q) = \Gamma/q^2$) with that for a rigid rod of the contour length of the native xanthan. Figure 10 shows the normalized plot of $D_{app}(q)/D_c(q=0)$. The experimental curve corresponds to the measurement at the lowest concentration. The rigid rod curve[37] shows only a very weak angular dependence and lies below the experimental curves for NX and PFX.[38] The "sliding-rod" approximation,[37,39] on the other hand, gives far too high values and overestimates the angular dependence. We then calculated the asymptotic plateau values for rods of the respective Kuhn lengths, using the Hammouda equations.[37] The plateau values apparently fit the general angular dependence of the experimental curves. These findings again confirm the wormlike chain behavior of the xanthan chains.

Acknowledgment. T.C. thanks the Institut für Makromolekulare Chemie for a personal grant. She is very grateful to all the colleagues of the laboratory, in particular, to Michael Eisele and Klaus Huber, for their help and fruitful discussions. K.K. is grateful to the Alexander von Humboldt Stiftung for an extention of his grant. The work was kindly supported by the Maizena Gesellschaft, Hamburg, and by the Deutsche Forschungsgemeinschaft within the scheme SFB 60.

Registry No. NX, 11138-66-2.

References and Notes

(1) Paradossi, G.; Brant, D. A. *Macromolecules* **1982**, *15*, 874.
(2) Schmidt, M.; Paradossi, G.; Burchard, W. *Makromol. Chem., Rapid Commun.* **1985**, *6*, 767.
(3) Koyama, R. *Phys. Soc. Jpn.* **1973**, *34*, 1029.
(4) Gupta, A. K.; Cotton, J. P.; Marchal, E.; Burchard, W.; Benoît, H. *Polymer* **1976**, *17*, 363.
(5) Hsu, B.; McWherter, C. A.; Brant, D. A.; Burchard, W. *Macromolecules* **1982**, *15*, 1350.
(6) Nordermeer, J. W. M.; Daryanani, R.; Janeschitz-Kriegl, H. *Polymer* **1975**, *16*, 359.
(7) Dentini, M.; Crescenzi, V.; Blasi, D. *Int. J. Biol. Macromol.* **1984**, *6*, 93.
(8) Holzwarth, G.; Ogletree, J. *Carbohydr. Res.* **1979**, *76*, 277.
(9) Sloneker, J. H.; Jeanes, A. *Can. J. Chem.* **1962**, *40*, 1604.
(10) Rinaudo, M.; Milas, M.; Lambert, F.; Vincendon, M. *Macromolecules* **1983**, *16*, 816.
(11) Bantle, S.; Schmidt, M.; Burchard, W. *Macromolecules* **1982**, *15*, 1604.
(12) Burchard, W. In *Applied Fibre Science*; Happey, F., Ed.; Academic: London, 1978; p 381.
(13) Kratochvil, P. In *Light Scattering from Polymer Solutions*; Huglin, M. B., Ed.; Academic: London, 1972; p 333.
(14) (a) Holtzer, A. *J. Polym. Sci.* **1955**, *17*, 432. (b) Casassa, E. F.; Eisenberg, H. *Adv. Protein Chem.* **1964**, *30*, 287.
(15) Berne, B. J.; Pecora, R. *Dynamic Light Scattering*, Wiley: New York, 1976.
(16) Koppel, D. E. *J. Chem. Phys.* **1972**, *57*, 4814.
(17) (a) Burchard, W.; Schmidt, M.; Stockmayer, W. H. *Macromolecules* **1980**, *13*, 580. (b) Burchard, W.; Schmidt, M.; Stockmayer, W. H. *Macromolecules* **1980**, *13*, 1265.
(18) Benoît, H.; Doty, P. *J. Phys. Chem.* **1953**, *57*, 958.
(19) Schmidt, M. *Macromolecules* **1984**, *17*, 553.
(20) Sato, T.; Kojima, S.; Norisuye, T.; Fujita, H. *Polym. J. (Tokyo)* **1984**, *16*, 423.
(21) Sato, T.; Norisuye, T.; Fujita, H. *Polym. J. (Tokyo)* **1984**, *16*, 341.
(22) (a) Yoshizaki, T.; Yamakawa, H. *J. Chem. Phys.* **1980**, *72*, 57. (b) Yoshizaki, T.; Yamakawa, H. *Macromolecules* **1980**, *13*, 633.
(23) Müller, G.; Lecourtier, J.; Chauveteau, G.; Allain, C. *Makromol. Chem., Rapid Commun.* **1984**, *5*, 203.
(24) (a) Yamakawa, H.; Fujii, H. *Macromolecules* **1974**, *7*, 128. (b) Yamakawa, H.; Fujii, H. *Macromolecules* **1973**, *6*, 407.
(25) Yanaki, T.; Norisuye, T.; Fujita, H. *Macromolecules* **1980**, *13*, 1462.
(26) Utiyama, H.; Sakato, K.; Ikehara, K.; Setsuiye, T.; Kurata, M. *Biopolymers* **1974**, *12*, 53.
(27) (a) Godfrey, J. E.; Eisenberg, H. *Biophys. Chem.* **1976**, *5*, 30. (b) Borochov, N.; Eisenberg, H. *Biopolymers* **1984**, *23*, 1757.
(28) Burchard, W. *Macromolecules* **1978**, *11*, 455.
(29) Agreement is observed with the experimental data for PFX when the physically reasonable value $d = 2.2$ nm is used, but for NX an 18% lower R_H is calculated by the Yamakawa–Fujii theory. An increase of the chain thickness by a factor of about 2 reduces the deviation to 8%, but the value is still too low. We can offer at present no explanation for this agreement in one case (PFX) and disagreement in the other (NX); however, we have to repeat here that d in the Yamakawa–Fujii theory gives no details on the physical nature of the hydrodynamic interaction. It appears conceivable that a differently strong binding of water may change the hydrodynamically effective chain thickness.
(30) Schmidt, M.; Stockmayer, W. H. *Macromolecules* **1984**, *17*, 509.
(31) (a) Pyun, C. W.; Fixman, M. *J. Chem. Phys.* **1964**, *41*, 937. (b) Yamakawa, H. *Modern Theory of Polymer Solutions*; Harper and Row: New York, 1971.
(32) Wilcoxon, J.; Schurr, J. M. *Biopolymers* **1983**, *22*, 849.
(33) Maeda, T.; Fujime, S. *Macromolecules* **1984**, *17*, 1157.
(34) de Gennes, P.-G. *Physics (Long Island City, N.Y.)* **1967**, *3*, 37.
(35) Akcasu, A. Z.; Benmouna, M.; Han, C. C. *Polymer* **1980**, *20*, 866.
(36) Hallett, F. R.; Nickel, B.; Craig, T. *Biopolymers* **1985**, *24*, 947.
(37) Hammouda, B. *Macromolecules* **1985**, *18*, 293.
(38) The shape function given by Hallett et al. is strictly valid only for $qL > 40$. In the present case the qL values ranged from 10 to 30, and this implies deviations to lower values of about 10%.
(39) Benmouna, M.; Akcasu, A. Z.; Daoud, M. *Macromolecules* **1980**, *13*, 1703.
(40) Coviello, T.; Burchard, W.; Dentini, M.; Crescenzi, V. *Macromolecules*, manuscript in preparation.
(41) Holzwarth, G. *Carbohydr. Res.* **1978**, *66*, 173.